IEEE Access
Multidisciplinary | Rapid Review | Open Access Journal

Received March 7, 2018, accepted April 3, 2018, date of publication April 9, 2018, date of current version May 9, 2018.

Digital Object Identifier 10.1109/ACCESS.2018.2824849

Online Path Planning of Autonomous UAVs for Bearing-Only Standoff Multi-Target Following in Threat Environment

HAO JIANG AND YUEQIAN LIANG
Seventh Research Division, Center for Information and Control, Beihang University, Beijing 100191, China
Corresponding author: Hao Jiang (031jianghao@gmail.com)

ABSTRACT The problem of steering multiple fixed-wing autonomous unmanned aerial vehicles (UAVs) to follow the multiple noncooperative and high agile surface targets at a specified standoff distance in a threat environment is studied. Two kinds of threats and missed detection of bearing-only sensors are considered. The average nonlinear least-square estimation method is proposed to acquire the position of the targets using noisy measurements, and then, the trajectories of the targets are approximated by the quadratic functions of time. Dummy targets of the same number as UAVs are created according to the task allocation result to achieve the optimal geometric configuration of the multiple cooperative UAVs. And a case-based guidance method is established to finally accomplish the multi-target standoff following mission on-line. Simulation experiments are given to assess the proposed method.

INDEX TERMS Standoff target following, autonomous system, path planning, threat environment, $\mathcal{K}$-coverage problem.

I. INTRODUCTION

Unmanned aerial vehicles (UAVs) have been employed extensively to assist and replace human beings to accomplish various work that involves difficulties and risks both in civilian and military areas during the last few decades. Because of the reliability and persistency, multiple low-cost UAVs are typically grouped as a system to cooperatively perform a designated task, and more will be benefited from the autonomy of the UAV system which requires the capabilities of detecting internal and external changes and of reacting to them in a safe and efficient manner without any human intervention [1]–[4].

Optimal path planning of the UAV system is always an essential consideration in such missions as target searching and exploring [5]–[8], strategical/tactical reconnaissance [9], [10], convoy protection [11], [12], target localization [13]–[15]. Target searching and exploring requires the UAV system to maximize the probability of detecting some unknown number of targets by the end of the mission, or equivalently to maximize the expected number of detected targets during the mission [5]–[7], and to find certain targets in minimum time in a certain bounded area [8], etc. In [9] multiple vehicle cooperative tactical reconnaissance was described as an optimal control problem with the Fisher information matrix (FIM) as the cost in the presence of risk zones and endpoint constraints, and the problem was then solved numerically in a receding horizon manner. The results shows how the triangulation and range reduction trade off in different cases. To prevent the cooperative surface vehicles (ground vehicles or ships) from ambushing or attacking by hidden forces, multiple UAVs can be formed to loiter around the surrounding environment to supply convoy protection [11], [12]. It is shown in [13]–[15] that the relative sensor-target geometric configuration can significantly affect the performance of the target localization algorithms. Martínez and Bullo proposed a motion coordination algorithm to steer the mobile sensor network to the optimal deployment they have derived [13]. The minimization of the lower bound of any unbiased estimator, i.e., the well-known Cramér-Rao lower bound (CRLB), which is equivalent to maximize the determinant of the FIM, is chosen as the optimality criterion in [14] to identify the optimal configuration of multiple identical sensor platforms when range-only, time-of-arrival or bearing-only sensors are used. Some interesting results were derived: there are infinite number of optimal configurations when the sensor number exceeds a certain value, and equal angular spacing about the target is not always the optimal configuration, etc. The optimal geometry of multiple heterogeneous passive sensors was also studied [15].

Optimal path planning schemes can mostly be classified into two categories. The first one is the configuration space approach, which depends on the decomposition of the task space and consists of cell decomposition method [16], roadmap method [17], [18], artificial potential method [19], [20], and so on. The second one is the evolutionary approach [21], [22], which employs varieties of evolutionary approaches, such as Genetic Algorithm (GA), Particle Swarm Optimization (PSO), Ant Colony Optimization (ACO), Simulated Annealing (SA), etc., to solve the formulated optimal problems. Detailed path planning schemes can be found in the book [23] and the survey papers [24], [25] and references therein.

Target following mission using the UAV system also relies much on the optimal path planning [1], [2], [11], [26]–[28]. If the surface target followed has no threat, UAVs can fly directly over it [1], [26], [27], otherwise the UAVs have to follow it from a certain standoff security distance [2], [11], [28]. The following problem of one target in the presence of threats, obstacles and restricted areas was addressed in [1] and [27]. The probabilistic threat exposure map (PTEM) was introduced to define various types of threats in a single framework, and a rule-based intelligent guidance algorithm was developed for real-time target following. The coordinated standoff target following was investigated in [2], [11], and [28] and the Lyapunov guidance vector fields were used to maintain the circular orbit of the UAV system around a moving target from a prescribed standoff radius and in the meantime the angular spacing between the UAVs.

The problem of following multiple noncooperative surface targets at a standoff distance using a team of autonomous UAVs in the presence of threats and missed detections is addressed in this paper. Methods are proposed to estimate, predict the positions of the targets, then allocate one target for each UAV and finally guide the UAVs to accomplish the follow mission. The main contributions are three aspects. Firstly with no knowledge of the target motion model in the noncooperative environment, the average nonlinear least-square estimation method (ANLSE) is presented to localize the targets from the sensed measurements at every sampling instant and then this localization is utilized to update the parameters of the approximated target trajectories which are quadratic functions of time and can be used to predict the target trajectories in the near future. Secondly considering the benefits of the optimal sensor-target geometric configurations in the literature, we introduce dummy targets of the same number as UAVs and attempt to deploy the UAVs ''optimally" surrounding the targets. The last and most important contribution is that a case-based guidance method is designed for the UAVs to cooperatively follow the targets. Compared with the previous-mentioned path planning methods, although the planned paths are not the optimal ones, the computational cost is very small. This is because the proposed method provides a quasi-analytical solution by virtue of 4 cases.

The remainder of the paper is structured as follows. The whole problem is specified in the next section. The problem is then resolved by the approach in section 3 which is comprised of six steps. Several simulation experiments are carried out in section 4 to illustrate the efficiency of the proposed approach. Some concluding remarks are then given in the last section.

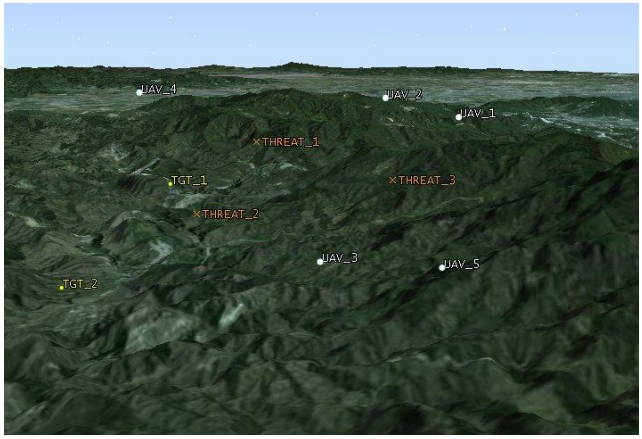

FIGURE 1. An example of the multi-target following problem with mountains, two targets, three threats and five UAVs.

II. PROBLEM FORMULATION

One example of the problem can be sketched as the scenario in Fig. 1.

Multiple noncooperative targets are moving in the considered surveillance region where different kinds of security threats (e.g., hills, air defences herein) may exist. Multiple autonomous UAVs are ordered to follow these targets as a team. These UAVs are supposed to avoid the security threats and stay a certain distance away from the targets considering their probable threat to the UAVs. The UAVs have to predict the motion of the targets before they make their own motion decisions because of the noncooperation of the targets. Modeling of the threat environment, devices and following capability of the UAVs and the target information collected by the UAVs are expatiated in the remainder of this section.

A. THREAT MODELING

All of the obstacles and restricted areas that cannot be entered, such as mountains, high buildings and some no-fly zones, etc., are named ''hard threat" here in this paper.

All of them are of certain shapes and sizes. One small enough ellipsoid which encompasses such a hard threat is chosen to model this hard threat. Every ellipsoid can be defined by its center $\mathcal{A}$ and its shape matrix $\mathcal{P}$ where $\mathcal{A} \in \mathbb{R}^3$ is a point in 3D space and $\mathcal{P} > 0$ is a 3×3 positive definite matrix. And the equation of this ellipsoid is actually $(\mathbf{p}-\mathcal{A})^T \mathcal{P}^{-1} (\mathbf{p}-\mathcal{A}) \leq 1$, where $\mathbf{p} = [x, y, z]^T$ represents the 3D UAV position. Define the following collision function

$$\mathcal{F}(\mathbf{p}) = 1 - (\mathbf{p}-\mathcal{A})^T \mathcal{P}^{-1} (\mathbf{p}-\mathcal{A}) . \tag{1}$$

It can be easily seen that not allowing a UAV to enter this hard threat is equivalent to $\mathcal{F}(\mathbf{p}) < 0$.

Remark 1: Here in this paper "shape matrix" means that the elements in the matrix $\mathcal{P}$ determine the shape of the ellipsoid. For example, letting diag(·) create diagonal matrix from a vector, if $\mathcal{P} = \text{diag}([r^2, r^2, r^2])$, then the ellipsoid is actually a sphere, and if $\mathcal{P} = \text{diag}([a^2, b^2, c^2])$, then the three axes of the ellipsoid are parallel to the axes of the coordinate system. And if the off-diagonal elements of $\mathcal{P}$ are not 0, then there exist nonzero angles between the three axes of the ellipsoid and the axes of the coordinate system.

Assume that there are $\mathcal{M}_1$ disconnected hard threats in the surveillance region considered herein and they are denoted by $\mathcal{H}_m = \{\mathcal{A}_m, \mathcal{P}_m\}$ for $m = 1, 2, ..., \mathcal{M}_1$. And the collision function corresponding to the m-th hard threat is $\mathcal{F}_m(\mathbf{p})$.

It may be not that easy to determine $\mathcal{A}_m$ and $\mathcal{P}_m$ for every hard threat in 3D space, so we then give the 2D description of a hard threat which is convenient when the UAVs are in the altitude-hold flight. For the m-th hard threat, an ellipse with its center located at $\mathcal{A}_m(z)$ and its shape defined by $\mathcal{P}_m(z)$ can be used as the hard threat model at altitude z. Note that these two functions with respect to the altitude z are a 2D vector and a 2×2 semi-positive definite matrix respectively and it means that no hard threat needs to avoid when $\mathcal{P}_m(z) = 0$, i.e., when z exceeds the height of the m-th 3D hard threat. The collision function related to $\mathcal{H}_m$ at altitude z can then be expressed as

$$\mathcal{F}_m(\mathbf{p}) = 1 - (\mathbf{p}_2 - \mathcal{A}_m(z))^T \mathcal{P}_m^{-1}(z) (\mathbf{p}_2 - \mathcal{A}_m(z)), \quad (2)$$

where $\mathbf{p}_2 = [x, y]^T$ is the horizontal position of a UAV.

Based on the defined model for the hard threats, the UAV at position $\mathbf{p}$ needs to satisfy $\mathcal{F}_m(\mathbf{p}) < 0$ for both the altitude-variant and altitude-invariant cases.

Another type of threats relates to the air defences, such as surface-to-air missiles and anti-aircraft artilleries. These threats are of no collision risks with the UAVs, and need to be avoided far away if possible. So we name this type of threats as "soft threat".

$\mathcal{M}_2$ soft threats are considered in the whole mission. Threat value of the m-th soft threat to the UAVs at altitude z is modeled as the following threat function

$$\mathcal{G}_m(\mathbf{p}) = \lambda(z) \exp\left[-\frac{1}{2}(\mathbf{p}_2 - \mathcal{B}_m(z))^T \mathcal{Q}_m^{-1}(z) (\mathbf{p}_2 - \mathcal{B}_m(z))\right], \quad (3)$$

where $\lambda(z)$ is the threat intensity related to the altitude z, $\mathcal{B}_m(z)$ can be interpreted as the site of the m-th soft threat, and $\mathcal{Q}_m(z) \geq 0$ is the corresponding threat range. Function $\mathcal{G}_m(\mathbf{p})$ can also be regarded as the probability of the event that a UAV located at $[x, y, z]^T$ is hit or destroyed by the m-th soft threat. If the difference of threat intensity at different altitudes is not considered, e.g., when the UAVs fly at altitudes that differs not too much, $\lambda(z)$ can be set to 1. The total threat of all the soft threats at the location $\mathbf{p}$ is then

$$\mathcal{G}(\mathbf{p}) = \sum_{m=1}^{\mathcal{M}_2} \mathcal{G}_m(\mathbf{p}). \quad (4)$$

The total threat value needs to be small for the UAV to stay as far away from soft threats as possible.

B. EMPLOYED UAVS

In consideration of the advantages in flight range, speed and reliability over rotorcrafts, fixed-wing UAVs are used more widely for target surveillance and following missions. They are therefore used as sensor platforms for multi-target following in this paper too.

Every UAV takes along a Global Positioning System (GPS) receiver with it to localize its own position and no navigation error is considered. One bearing-only sensor is mounted on each UAV, and all of the sensors have been synchronized at the beginning of the mission. The UAVs are equipped with low-level flight control systems that can provide roll, pitch, and yaw stability of the aircrafts and velocity tracking and altitude-hold functions as well [11]. Explicit speed, turn rate and climb rate can be used as the control inputs. One of the UAVs (UAV 1 herein) is chosen as the processing center which can process various data (e.g., bearing measurements received from the other UAVs) and then share the results with the other UAVs through communication. No communication range is limited here since this can be resolved by additional communication relays.

The maneuverability of surface targets outperforms most fixed-wing UAVs since they can stop and turn around very quickly without minimum speed and comparatively large turn radius constraints. The kinematic model of UAV s is given by

$$\begin{cases} \dot{x}_s = u_{1s} \cos\psi_s \\ \dot{y}_s = u_{1s} \sin\psi_s \\ \dot{\psi}_s = u_{2s} \\ \dot{z}_s = u_{3s} \end{cases} \quad (5)$$

where $s = 1, 2, \ldots, S$ with S being the number of UAVs used for target following, ψ_s is the heading angle of UAV s, and the three control variables u_{1s}, u_{2s} and u_{3s} are respectively the commanded air speed, turning rate and climb rate. No background wind is present during the whole mission. Denote $\mathbf{u}_s = [u_{1s}, u_{2s}, u_{3s}]^T$. The constraints on these commanded variables and the acceleration a_s are given as

$$0 < V_{s,min} \leq u_{1s} \leq V_{s,max}, \quad (6)$$

$$a_{s,min} \leq a_s \leq a_{s,max}, \quad (7)$$

$$\omega_{s,min} \leq u_{2s} \leq \omega_{s,max}, \quad (8)$$

$$\gamma_{s,min} \leq u_{3s} \leq \gamma_{s,max}. \quad (9)$$

Every UAV can be modeled as a moving hard threat to avoid possible collisions between two UAVs. Usually a security sphere with radius R_s can be defined for UAV s to achieve the collision avoidance. The collision function related to UAVs s_1 and s_2 can be expressed by

$$\mathcal{C}(\mathbf{p}_{s_1}, \mathbf{p}_{s_2}) = (R_{s_1} + R_{s_2})^2 - \|\mathbf{p}_{s_1} - \mathbf{p}_{s_2}\|^2. \quad (10)$$

It requires that $\mathcal{C}(\mathbf{p}_{s_1}, \mathbf{p}_{s_2}) \leq 0$ to ensure the security of UAVs s_1 and s_2. If the UAVs are all keeping their altitude unchanged during the mission, which can be achieved by simple proportional feedback control of climb rate, $u_{3s} = -K_{z,s}(z_s - z_{s,des})$, where $K_{z,s}$ is the proportional gain and

$z_{s,des}$ is the desired altitude, then the collision avoidance problem can be out of the question by letting different UAVs fly at different altitudes.

C. SENSOR MEASUREMENTS

It is assumed that N targets have been identified when the mission initiates. If perfect detection and no clutter are considered, noisy bearing angles from UAV s to target n can be given as

$$\begin{aligned}\mathbf{z}_{sn} &= \begin{bmatrix}\theta_{sn}\\ \phi_{sn}\end{bmatrix} = \mathbf{h}_s\left(\tilde{\mathbf{p}}_n\right) + \mathbf{e}_s \\ &= \begin{bmatrix}\tan^{-1}\left(\frac{\tilde{y}_n - y_s}{\tilde{x}_n - x_s}\right)\\ \tan^{-1}\left(\frac{\tilde{z}_n - z_s}{\sqrt{(\tilde{x}_n - x_s)^2 + (\tilde{y}_n - y_s)^2}}\right)\end{bmatrix} + \begin{bmatrix}\mu_s\\ \nu_s\end{bmatrix}, \quad (11)\end{aligned}$$

where $s = 1, 2, \ldots, S$, $n = 1, 2, \ldots, N$, θ_{sn} and ϕ_{sn} are the two measured bearing angles from sensor s to target n, i.e., the azimuth angle and elevation angle respectively, μ_s and ν_s are the corresponding measurement noises which are assumed to be mutually independent among different sensors and Gaussian distributed with zero means and variances σ_μ^2 and σ_ν^2 respectively, and $\tan^{-1}(\cdot)$ is the four-quadrant inverse tangent function. $\mathbf{p}_s = [x_s, y_s, z_s]^T$ and $\tilde{\mathbf{p}}_n = [\tilde{x}_n, \tilde{y}_n, \tilde{z}_n]^T$ are used to denote the positions of sensor s and target n respectively.

Sensor detection turns out to be imperfect in practice which is typically known as missed detection. This imperfection may result from geomorphic feature, local weather, occlusion and even sensor type, and is usually characterized by sensor detection probability. Here in this paper the detection probability of sensor s, Ψ_s, is assumed to be related to the sensor-target range and reduces to zero if the line-of-sight from a UAV to a target is blocked by the terrain. Specifically the detection probability Ψ_s is defined as

$$\Psi_s(\mathbf{p}) = \begin{cases}0, & \text{if line segment } \mathbf{p}_s\mathbf{p} \text{ and}\\ & \text{the terrain intersect}\\ \exp\left(-\frac{r_s}{r_0}\right), & \text{otherwise}\end{cases} \quad (12)$$

In Eq. (12) $r_s = \|\mathbf{p} - \mathbf{p}_s\|$ with $\|\cdot\|$ being the 2-norm operator is the range between sensor s and the emitting source located at $\mathbf{p}$, and r_0 is a reference range to characterize the sensor detection capability.

III. METHODOLOGY

In this section we elaborate the method to accomplish the bearing-only standoff multi-target following mission using autonomous UAVs. This method consists of 6 steps, which achieve the data association, target state estimation, target trajectory prediction, task allocation, UAV cooperation and UAV guidance functions respectively. The diagram of the solution to the whole mission is illustrated in Fig. 2.

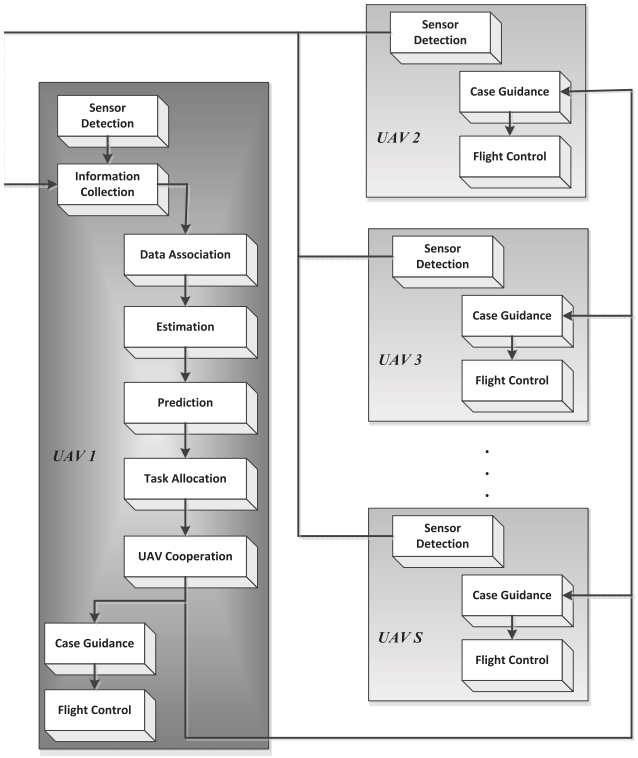

FIGURE 2. The diagram of the solution to the whole multi-target following mission.

A. STEP 1: SEQUENTIAL 2D ASSIGNMENT METHOD FOR DATA ASSOCIATION

The presence of missed detection and multiple targets induces the data association problem which requires us to determine the emitting origin of every sensor measurement [29], [30].

It is assumed that the mission starts at time t_0, ends at t_f and the sensors can obtain the bearing measurements every Δt seconds. We denote the measurements collected by sensor s at the current time t_k as

$$\mathbf{Z}_s(k) = \left\{\mathbf{z}_{s0}(k), \mathbf{z}_{s1}(k), \mathbf{z}_{s2}(k), \ldots, \mathbf{z}_{sN_s}(k)\right\}, \quad (13)$$

where dummy measurement $\mathbf{z}_{s0}(k)$ is introduced to represent missed detections. That is, target n which is associated with $\mathbf{z}_{s0}(k)$ is not detected by sensor s because of the imperfect detection as explained earlier. N_s is the actual number of nondummy returns received by sensor s. We further denote the S-tuple of measurements, $\left\{\mathbf{z}_{1i_1}(k), \mathbf{z}_{2i_2}(k), \ldots, \mathbf{z}_{Si_S}(k)\right\}$, which is composed of only one measurement (dummy or nondummy) from each sensor, as $\mathbf{Z}_{i_1 i_2 \cdots i_S}(k)$.

Under the assumption that each measurement originates from only one source and each sensor obtains at most one measurement from each target, data association problem herein can be formulated as a generalized multi-dimensional assignment (MDA) problem [31], [32].

The generalized MDA problem is a well-known NP hard problem when $S \geq 3$, and its suboptimal solution can be obtained by first successively relaxing the original problem using Lagrangian multipliers to a two-dimensional

assignment problem which can be optimally solved by several methods, e.g., the auction method [33], and then enforcing the constraints one by one and updating the Lagrangian multipliers in the meantime until all the constraints are added [29], [30]. This process continues until the gap between the primal cost and the dual cost is small enough, which indicates the acquirement of the suboptimal solution.

Instead of the multi-dimensional method [29], [30], the approximated sequential 2D assignment method given in [32], is applied here to address the data association problem.

B. STEP 2: ANLSE FOR ESTIMATION

After the association every target n is associated with an S-tuple measurement $\mathbf{Z}^{(n)}_{i_1 i_2 \cdots i_S}(k)$. If at least two nondummy measurements are included in this S-tuple measurement, then the current position of the target can be estimated by the following ANLSE method as $\hat{\tilde{\mathbf{p}}}_n(k)$.

Assume that J ($2 \le J \le S$) nondummy measurements are in $\mathbf{Z}^{(n)}_{i_1 i_2 \cdots i_S}(k)$, and they can form a nondummy J-tuple measurement

$$\mathbf{Z}^{(n)}_{i_{j_1} i_{j_2} \cdots i_{j_J}}(k) = \left\{ \mathbf{z}_{j_1 i_{j_1}}(k), \mathbf{z}_{j_2 i_{j_2}}(k), \ldots, \mathbf{z}_{j_J i_{j_J}}(k) \right\}. \quad (14)$$

Stack these nondummy measurements as $\mathbf{z}_n(k) = \left[\mathbf{z}^T_{j_1 i_{j_1}}(k), \mathbf{z}^T_{j_2 i_{j_2}}(k), \ldots, \mathbf{z}^T_{j_J i_{j_J}}(k) \right]^T$. If two arbitrary measurements are selected from the J-tuple measurement $\mathbf{Z}^{(n)}_{i_{j_1} i_{j_2} \cdots i_{j_J}}(k)$, there are $M = \binom{J}{2}$ different combinations. The m-th combination can be denoted as $\left\{ \mathbf{z}_{j_{m_1} i_{j_{m_1}}}(k), \mathbf{z}_{j_{m_2} i_{j_{m_2}}}(k) \right\}$. From this combination an initial estimation of the target's position $\hat{\tilde{\mathbf{p}}}^{(m,0)}_n(k)$ can be given by (15)–(17), as shown at the bottom of the next page.

This initial position estimation can be used to obtain an estimation for target n through the following nonlinear least-square estimation (NLSE) iteration

$$\begin{aligned} \hat{\tilde{\mathbf{p}}}^{(m,l+1)}_n(k) = \hat{\tilde{\mathbf{p}}}^{(m,l)}_n(k) &+ \left[\left(\mathbf{H}^{(l)} \right)^T \mathbf{R}^{-1} \mathbf{H}^{(l)} \right]^{-1} \left(\mathbf{H}^{(l)} \right)^T \\ &\times \mathbf{R}^{-1} \left[\mathbf{z}_n(k) - \mathbf{h}\left(\hat{\tilde{\mathbf{p}}}^{(m,l)}_n(k) \right) \right], \end{aligned} \quad (18)$$

where $l = 0, 1, 2, \ldots, L_{max}$, $\mathbf{h}(\cdot)$ is the stack of the j_1-th, j_2-th, $\ldots$, j_J-th measurement functions, $\mathbf{R}$ is the corresponding noise covariances, and $\mathbf{H}^{(l)}$ is the stack of the Jacobian matrices of the corresponding sensors evaluated at $\hat{\tilde{\mathbf{p}}}^{(m,l)}_n(k)$.

If $\left\| \hat{\tilde{\mathbf{p}}}^{(m,l+1)}_n(k) - \hat{\tilde{\mathbf{p}}}^{(m,l)}_n(k) \right\|$ is less than one given small number ε, then the iteration stops. Otherwise the iteration continues until $l = L_{max}$ where L_{max} is a preset integer. We are assumed to obtain $\hat{\tilde{\mathbf{p}}}^{(m,l_m)}_n(k)$ ($l_m \le L_{max}$) through the iteration at last. If $\left\| \hat{\tilde{\mathbf{p}}}^{(m,l_m)}_n(k) - \hat{\tilde{\mathbf{p}}}^{(m,l_m-1)}_n(k) \right\| > \varrho$ where ϱ is a given proper large number, then we say that the iteration initialized with $\hat{\tilde{\mathbf{p}}}^{(m,0)}_n(k)$ diverges.

We do the above NLSE iteration for every $\hat{\tilde{\mathbf{p}}}^{(m,0)}_n(k)$ which corresponds to the m-th two-element combination of $\mathbf{Z}^{(n)}_{i_{j_1} i_{j_2} \cdots i_{j_J}}(k)$ and in the meantime determine the convergence of them. If none of the M NLSE iterations converges, we let

$$\hat{\tilde{\mathbf{p}}}_n(k) = \frac{1}{M} \sum_{m=1}^{M} \hat{\tilde{\mathbf{p}}}^{(m,0)}_n(k). \quad (19)$$

Otherwise the position estimation of target n is chosen as the average of the estimation of all the convergent NLSE iterations, i.e.,

$$\hat{\tilde{\mathbf{p}}}_n(k) = \left(\sum_{m=1}^{M} c_m \right)^{-1} \sum_{m=1}^{M} c_m \hat{\tilde{\mathbf{p}}}^{(m,l_m)}_n(k), \quad (20)$$

where c_m is an indicator to represent the convergence of the m-th NLSE iteration and is given by

$$c_m = \begin{cases} 0, & \text{if } \left\| \hat{\tilde{\mathbf{p}}}^{(m,l_m)}_n(k) - \hat{\tilde{\mathbf{p}}}^{(m,l_m-1)}_n(k) \right\| > \varrho \\ 1, & \text{otherwise} \end{cases} \quad (21)$$

This ends the ANLSE with the position estimation $\hat{\tilde{\mathbf{p}}}_n(k)$.

C. STEP 3: SECOND-ORDER TRAJECTORY APPROXIMATION FOR PREDICTION

The positions and velocities of the targets at future time instants should be predicted to complete the target following mission. We assume that the trajectory of target n can be approximated by the following quadratic function of time t

$$\tilde{\mathbf{p}}_n(t) = \tilde{\mathbf{p}}_{n0} + (t - t_0)\, \tilde{\mathbf{v}}_{n0} + \frac{(t - t_0)^2}{2}\, \tilde{\mathbf{a}}_{n0} = \mathbf{A}(t) \Theta_n, \quad (22)$$

where $\Theta_n = \left[\tilde{\mathbf{p}}^T_{n0} \;\; \tilde{\mathbf{v}}^T_{n0} \;\; \tilde{\mathbf{a}}^T_{n0} \right]^T$ is the approximated trajectory parameters to be determined, and the time-dependent matrix $\mathbf{A}(t)$ is $\left[\mathbf{I}_3 \;\; (t - t_0)\mathbf{I}_3 \;\; \frac{(t-t_0)^2}{2} \mathbf{I}_3 \right]$ with $\mathbf{I}_3$ being the 3×3 identity matrix. Taking the derivative of Eq. (22) with respect to time t, we have

$$\tilde{\mathbf{v}}_n(t) = \tilde{\mathbf{v}}_{n0} + (t - t_0)\, \tilde{\mathbf{a}}_{n0} = \mathbf{B}(t) \Theta_n, \quad (23)$$

where $\mathbf{B}(t) = [\mathbf{0}_{3\times 3} \;\; \mathbf{I}_3 \;\; (t - t_0)\mathbf{I}_3]$. This can be used to determine the velocity vector of target n.

Only the latest L (≥ 3) steps of collected measurements are assumed to influence the updating of the current trajectory parameters $\Theta_n(k)$. Stacking the estimated positions of the latest L_1 steps, we have

$$\begin{bmatrix} \hat{\tilde{\mathbf{p}}}_n(k - L_1 + 1) \\ \hat{\tilde{\mathbf{p}}}_n(k - L_1 + 2) \\ \vdots \\ \hat{\tilde{\mathbf{p}}}_n(k) \end{bmatrix} = \begin{bmatrix} \mathbf{A}(k - L_1 + 1) \\ \mathbf{A}(k - L_1 + 2) \\ \vdots \\ \mathbf{A}(k) \end{bmatrix} \Theta_n(k), \quad (24)$$

where $L_1 = \min\{L, k\}$. Rewrite Eq. (24) as $\mathscr{P}_n(k) = \mathscr{A}(k)\Theta_n(k)$, then the approximated parameters of the current step can be given by

$$\Theta_n(k) = \left[\mathscr{A}^T(k) \mathscr{A}(k) \right]^{-1} \mathscr{A}^T(k)\, \mathscr{P}_n(k). \quad (25)$$

It needs to be noted that if less than two sensors detect target n at the current time, then no estimation can be obtained

using the ANLSE. So we let $\Theta_n(k) = \Theta_n(k-1)$ in this case. Then the current estimation can be attained by use of $\Theta_n(k)$. And because of the same reason, all the targets are assumed to be detected by at least two sensors at the first three time instants $(t_0, t_0 + \Delta t, t_0 + 2\Delta t)$ to successfully initiate the trajectory approximation.

Once we have $\Theta_n(k)$, the positions and velocities of target n at recent times can be approximated. Especially the predicted position and velocity vector of target n at the next time instant can be computed as

$$\hat{\tilde{\mathbf{p}}}_n(k+1|k) = \mathbf{A}(t_{k+1})\Theta_n(k), \tag{26}$$
$$\hat{\tilde{\mathbf{v}}}_n(k+1|k) = \mathbf{B}(t_{k+1})\Theta_n(k). \tag{27}$$

D. STEP 4: 2D ASSIGNMENT METHOD FOR TASK ALLOCATION

Multiple sensors, especially in the case of passive ones, imperfect detection and sensor range constraints, should be allocated to follow one target, which is known as $\mathcal{K}$-coverage problem and adopted here in this paper. As mentioned before N targets are confirmed at the initial of the mission and none of the newly-discovered targets are considered. And this requires that $S \geq N\mathcal{K}$.

The UAVs can be allocated according to their minimum intercepting time [11] $d_{sn}(k)$ timing from the current step t_k, i.e.,

$$d_{sn}(k) = \min\ t_e, \tag{28}$$

subject to Eqs. (5)-(9) and

$$\left\| \tilde{\mathbf{p}}_n(t_k + t_e) - \mathbf{p}_s(t_k + t_e) \right\| = 0. \tag{29}$$

Alternatively an approximation of $d_{sn}(k)$ as $\left\| \tilde{\mathbf{p}}_n(k+1|k) - \mathbf{p}_s(k) \right\|$ can be taken to avoid solving the optimal control problem (28) subject to (5)-(9) and (29).

Then the $\mathcal{K}$-coverage problem used for task allocation can be formulated as

$$\min_{\delta_{sn}(k)} \sum_{s=1}^{S} \sum_{n=1}^{N} d_{sn}(k)\, \delta_{sn}(k), \tag{30}$$

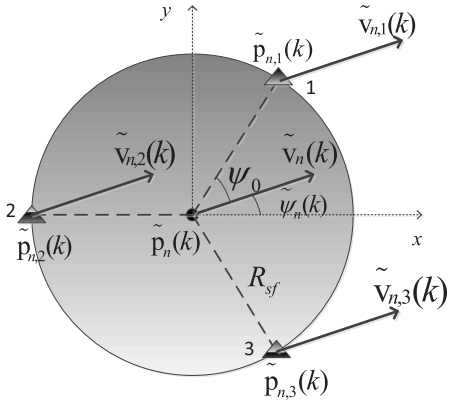

FIGURE 3. Dummy targets corresponding to target n with $S_n = 3$.The filled circle denotes the true target, and the three filled triangles are the three dummy targes.

subject to

$$\begin{cases} \sum_{n=1}^{N} \delta_{sn}(k) = 1, & s = 1, 2, \ldots, S \\ \sum_{s=1}^{S} \delta_{sn}(k) \geq \mathcal{K}, & n = 1, 2, \ldots, N \end{cases} \tag{31}$$

where $\delta_{sn}(k)$ is a binary variable with $\delta_{sn}(k) = 1$ meaning that UAV s is allocated to follow target n at the current time. This is a 2D assignment problem and can also be solved optimally by the auction algorithm [33] after some simple transformation.

E. STEP 5: DUMMY TARGET CREATING FOR UAV COOPERATION

From the task allocation solution we can determine the number of UAVs which are used to follow every target n, $n = 1, 2, \ldots, N$. We denote this number as S_n $(\geq \mathcal{K})$. To cooperatively follow every target n at a standoff distance and take the influence of the sensor-target geometric configuration on target localization and tracking into consideration, every target n is duplicated as S_n dummy targets (Fig. 3).

Based on the optimal geometric configuration results given in [14], the positions and velocities of these dummy targets

$$\hat{\tilde{x}}_n^{(m,0)}(k) = \frac{\left[x_{j_{m_1}} \tan\left(\theta_{j_{m_1}n}\right) - x_{j_{m_2}} \tan\left(\theta_{j_{m_2}n}\right)\right] - \left(y_{j_{m_1}} - y_{j_{m_2}}\right)}{\tan\left(\theta_{j_{m_1}n}\right) - \tan\left(\theta_{j_{m_2}n}\right)}, \tag{15}$$

$$\hat{\tilde{y}}_n^{(m,0)}(k) = \frac{\left[y_{j_{m_2}} \tan\left(\theta_{j_{m_1}n}\right) - y_{j_{m_1}} \tan\left(\theta_{j_{m_2}n}\right)\right] + \left(x_{j_{m_1}} - x_{j_{m_2}}\right) \tan\left(\theta_{j_{m_1}n}\right) \tan\left(\theta_{j_{m_2}n}\right)}{\tan\left(\theta_{j_{m_1}n}\right) - \tan\left(\theta_{j_{m_2}n}\right)}, \tag{16}$$

$$\hat{\tilde{z}}_n^{(m,0)}(k) = z_{j_{m_1}} + \tan\left(\phi_{j_{m_1}n}\right) \left| \frac{\left(x_{j_{m_1}} - x_{j_{m_2}}\right) \sin\left(\theta_{j_{m_2}n}\right) - \left(y_{j_{m_1}} - y_{j_{m_2}}\right) \cos\left(\theta_{j_{m_2}n}\right)}{\sin\left(\theta_{j_{m_1}n} - \theta_{j_{m_2}n}\right)} \right|. \tag{17}$$

can be computed as ($i = 1, 2, \ldots, S_n$)

$$\tilde{\mathbf{p}}_{n,i}(k) = \tilde{\mathbf{p}}_n(k) + R_{sf} \begin{bmatrix} \cos\left(\tilde{\psi}_n(k) + \psi_0 + (i-1)\,\delta\psi\right) \\ \sin\left(\tilde{\psi}_n(k) + \psi_0 + (i-1)\,\delta\psi\right) \end{bmatrix} \tag{32}$$

$$\tilde{\mathbf{v}}_{n,i}(k) = \tilde{\mathbf{v}}_n(k) \tag{33}$$

where

$$\delta\psi = \begin{cases} \pi/2, & \text{if } S_n = 2 \\ 2\pi/S_n, & \text{if } S_n > 2 \end{cases} \tag{34}$$

and R_{sf} is the selected standoff distance. ψ_0 is a designed parameter, denoting the line-of-sight angle from the position of target n to the first dummy target minus the heading angle of target n.

After we have these dummy targets, every UAV can be commanded to follow one of them. The position and velocity of the dummy target allocated to UAV s are denoted as $\tilde{\mathbf{q}}_s(k)$ and $\tilde{\mathbf{w}}_s(k)$ respectively hereafter, similarly the estimations and predictions.

F. STEP 6: CASE-BASED GUIDANCE METHOD FOR TARGET FOLLOWING

The objectives of the target following mission include three ones: avoiding the hard threats; flying as close to the allocated dummy target as possible; staying far away from the soft threats if possible.

In the ideal case that we know exactly the trajectories of all the targets, the optimal paths for the UAVs can be determined by solving the following optimal control problem

$$\min_{\{\mathbf{p}_s(t),\mathbf{u}_s(t)\}} \int_{t_0}^{t_f} \left[\alpha \sum_{s=1}^{S} \left\| \mathbf{p}_s(t) - \tilde{\mathbf{q}}_s(t) \right\| + \kappa\beta \sum_{s=1}^{S} \mathcal{G}(\mathbf{p}_s(t)) \right] \mathrm{d}t, \tag{35}$$

subject to Eqs. (5)-(9) and

$$\mathcal{F}_m(\mathbf{p}_s(t)) < 0, \quad \text{for } s = 1, 2, \ldots, S;\ m = 1, 2, \ldots, \mathcal{M}_1. \tag{36}$$

The parameters $\alpha > \beta \geq 0$ in Eq. (35) satisfy $\alpha + \beta = 1$, standing for the tradeoff between the second and third objectives stated earlier, and $\kappa > 0$ is a scaling factor to equalize the order of the two terms in the integral.

The optimal problem can be considered in a receding horizon manner

$$\min_{\{\mathbf{p}_s(t),\mathbf{u}_s(t)\}} \int_{t_k}^{t_{k+M}} \left[\alpha \sum_{s=1}^{S} \left\| \mathbf{p}_s(t) - \tilde{\mathbf{q}}_s(t) \right\| + \kappa\beta \sum_{s=1}^{S} \mathcal{G}(\mathbf{p}_s(t)) \right] \mathrm{d}t, \tag{37}$$

where M is the length of the time horizon. Since $\tilde{\mathbf{p}}_n(t)$ and therefore $\tilde{\mathbf{q}}_s(t)$ is unknown to the mission designers, the current trajectory parameter $\Theta_n(k)$ can be used to predict the future trajectory corresponding to the time domain $[t_k, t_k + M\Delta t]$. Especially M can be taken to 1 for the prediction may be inaccurate when the time domain is too large.

The optimal control problem Eq. (35) or (37) with constraints (5)-(9) and (36) can be solved by indirect methods [34] and direct methods [35]–[37] which are both time-consuming though. Taking the Gauss pseudospectral method as an example [35], [36], if $\mathcal{L}$ Legendre-Gauss points are used, then at every time step a nonlinear programming problem with $6\mathcal{L}$ variables has to be solved when the altitude-hold flight is constrained for all the UAVs. This is usually hard to be implemented real-timely since $\mathcal{L}$ usually cannot be too small to ensure the accuracy of the solution. A new case-based suboptimal method is proposed here to trade off the optimality and the real-time performance when the UAVs are controlled to stay at the same altitude throughout the mission.

Firstly to prevent the UAVs from being hit or destroyed by soft threats, we set a threat threshold $\mathcal{G}_{TH}(\alpha)$ according to the mission parameter α. That is, during the whole mission, every UAV is prohibited from entering the zone where the soft threat value exceeds $\mathcal{G}_{TH}(\alpha)$.

The current state of UAV s is assumed to be

$$\begin{aligned} \mathbf{x}_s(k) &= \left[\mathbf{p}_s^T(k)\ \mathbf{v}_s^T(k)\right]^T \\ &= \left[x_s(k)\ y_s(k)\ z_s(k)\ v_{xs}(k)\ v_{ys}(k)\ v_{zs}(k)\right]^T, \end{aligned} \tag{38}$$

where $z_s(k) \equiv z_s$ and $v_{zs}(k) \equiv 0$ for the altitude-hold case. And the speed and heading angle are denoted as $V_s(k)$ and $\psi_s(k)$ respectively.

It can be easily seen from Eqs. (6)-(9) that the possible heading angle range and speed range are

$$\mathcal{V}_{\psi,s}(k) = \left[\psi_s(k) + \omega_{s,min}\,\Delta t, \quad \psi_s(k) + \omega_{s,max}\,\Delta t\right], \tag{39}$$

and

$$\begin{aligned} \mathcal{V}_{V,s}(k) = \big[&\max\left\{V_s(k) + a_{s,min}\,\Delta t, V_{s,min}\right\}, \\ &\min\left\{V_s(k) + a_{s,max}\,\Delta t, V_{s,max}\right\}\big], \end{aligned} \tag{40}$$

respectively after one time step Δt.

We let

$$r_s(k) = \left\| \hat{\tilde{\mathbf{q}}}_s(k+1|k) - \mathbf{p}_s(k) \right\|, \tag{41}$$

$$\Delta V_s(k) = \left\| \hat{\tilde{\mathbf{w}}}_s(k+1|k) \right\| - V_s(k), \tag{42}$$

and the angle

$$\psi_{c,s}(k) = \tan^{-1}\left(\frac{\hat{\tilde{y}}_{\mathbf{q}_s}(k+1|k) - y_s(k)}{\hat{\tilde{x}}_{\mathbf{q}_s}(k+1|k) - x_s(k)} \right), \tag{43}$$

denotes the line-of-sight angle from the current position of UAV s to the predicted position of allocated target at the next time instant.

The furthest two points that UAV s can reach with its current speed in the maximum and minimum turning rates

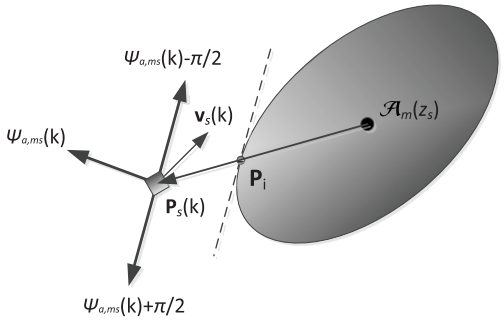

FIGURE 4. The heading angle range that makes UAV *s* fly away from hard threat *m*. The filled circle denotes the center of the hard threat, the filled ellipse denotes the hard threat, and the filled square is the position of UAV *s*.

are respectively

$$\mathbf{p}_s^{(l)}(k) = \begin{bmatrix} x_s(k) \\ y_s(k) \\ z_s \end{bmatrix} + \frac{V_s(k)}{\omega_{s,max}} \begin{bmatrix} \sin\left(\psi_s(k) + \omega_{s,max}\, t_\perp\right) - \sin\left(\psi_s(k)\right) \\ -\cos\left(\psi_s(k) + \omega_{s,max}\, t_\perp\right) + \cos\left(\psi_s(k)\right) \\ 0 \end{bmatrix}, \tag{44}$$

and

$$\mathbf{p}_s^{(r)}(k) = \begin{bmatrix} x_s(k) \\ y_s(k) \\ z_s \end{bmatrix} + \frac{V_s(k)}{\omega_{s,min}} \begin{bmatrix} \sin\left(\psi_s(k) + \omega_{s,min}\, t_\perp\right) - \sin\left(\psi_s(k)\right) \\ -\cos\left(\psi_s(k) + \omega_{s,min}\, t_\perp\right) + \cos\left(\psi_s(k)\right) \\ 0 \end{bmatrix}, \tag{45}$$

where $t_\perp = \pi/(2\omega_{s,max})$ is the time for the UAV to make a 90° turn with its maximum turning rate.

We then compute two heading angle ranges, $\mathcal{V}_{a,ms}(k)$ and $\mathcal{V}_{min,s}(k)$.

If there exists a $m \in \{1, 2, \ldots, \mathcal{M}_1\}$ that makes $\mathcal{F}_m(\mathbf{p}_s^{(l)}(k)) \geq 0$ or $\mathcal{F}_m(\mathbf{p}_s^{(r)}(k)) \geq 0$, then we take

$$\mathcal{V}_{a,ms}(k) = \left[\psi_{a,ms}(k) - \pi/2, \quad \psi_{a,ms}(k) + \pi/2\right], \tag{46}$$

where $\psi_{a,ms}(k)$ is one of the perpendicular directions, which is closer to the direction of vector $\overrightarrow{\mathcal{A}_m(z_s)\mathbf{p}_s(k)}$, to the tangential of the ellipse $\{\mathcal{A}_m(z_s), \mathcal{P}_m(z_s)\}$ at the points where this ellipse and the line through $\mathbf{p}_s(k)$ and $\mathcal{A}_m(z_s)$ intersect (See Fig. 4).

The calculation of $\psi_{a,ms}(k)$ is given in Appendix A. Otherwise we let $\mathcal{V}_{a,ms}(k) = [0, 2\pi)$.

If we have $\mathcal{G}(\mathbf{p}_s^{(l)}(k)) \geq \mathcal{G}_{TH}(\alpha)$ or $\mathcal{G}(\mathbf{p}_s^{(r)}(k)) \geq \mathcal{G}_{TH}(\alpha)$, then the following angle

$$\psi_{min,s}(k) = \tan^{-1}\left(\frac{-\partial\mathcal{G}(\mathbf{p})/\partial y}{-\partial\mathcal{G}(\mathbf{p})/\partial x}\Big|_{\mathbf{p}=\mathbf{p}_s(k)}\right), \tag{47}$$

where ∂ is the partial derivative operator, is first obtained, and $\mathcal{V}_{min,s}(k)$ is given as

$$\mathcal{V}_{min,s}(k) = \left[\psi_{min,s}(k) - \pi/2, \quad \psi_{min,s}(k) + \pi/2\right]. \tag{48}$$

Otherwise we take $\mathcal{V}_{min,s}(k) = [0, 2\pi)$.

Then another two angle ranges can be achieved as

$$\mathcal{V}_{CAHR,s}(k) = \mathcal{V}_{a,ms}(k) \cap \mathcal{V}_{\psi,s}(k), \tag{49}$$

$$\mathcal{V}_{TAHR,s}(k) = \mathcal{V}_{CAHR,s}(k) \cap \mathcal{V}_{min,s}(k). \tag{50}$$

Four cases are considered here to complete the target following mission.

Case 1: $\mathcal{V}_{CAHR,s}(k) = \emptyset$. In this case the probability of the collision between UAV *s* and hard threat *m* is very large if UAV *s* maintains its current speed. To avoid the possible collision, UAV *s* should decelerate to the greatest degree to turn around as fast as possible.

Case 2: $\mathcal{V}_{CAHR,s}(k) \neq \emptyset$ but $\mathcal{V}_{TAHR,s}(k) = \emptyset$. UAV *s* will probably enter the high-risk zone if no change of the speed is done. It requires UAV *s* to slow down to the best of its ability too.

Case 3: $\mathcal{V}_{CAHR,s}(k) \neq \emptyset$, $\mathcal{V}_{TAHR,s}(k) \neq \emptyset$, but $r_s(k) > r_{TH}$. Here r_{TH} is a designed parameter to indicate the closeness of UAV to the target. If their distance is less than r_{TH}, then they are deemed to be close enough. In this case, UAV *s* can avoid collision with all the hard threats and not enter the high-risk zones by tuning the heading angle, but the distance between UAV *s* and its allocated target is not small enough. So the UAV should head for the target as fast as possible.

Case 4: $\mathcal{V}_{CAHR,s}(k) \neq \emptyset$, $\mathcal{V}_{TAHR,s}(k) \neq \emptyset$, and $r_{sn}(k) \leq r_{TH}$. The difference from *Case 3* is that UAV *s* and its allocated target is close enough in this case. And the second and third objectives should trad off according to the mission parameter α.

To achieve the objectives of the target following mission, the desired heading angle and speed and their admissible ranges at the current time t_k can be specified according to these four cases. This is shown in Table 1. K_V and K_r are the proportional gains for the speed and position errors respectively for *Case 4*. The commanded heading angle and speed signals are chosen as the closest value to the desired one in the admissible domain. And the first-order transfer function is used as the low-level controller on the UAVs to track the given commanded signals.

IV. SIMULATION RESULTS

A. SIMULATION SETTINGS

Two high agile and noncooperative targets are designed to be followed by multiple UAVs each equipped with one bearing-only sensor in this section. Here "high agile" means that the maneuverability of the surface targets is much better than that of the fixed-wing UAVs, in the sense that the targets can stop and make turns with very small turning radius. The times and time step of the following mission are taken to be $t_0 = 0$, $t_f = 1300$s and $\Delta t = 3$s respectively.

The two targets can accelerate, decelerate, stop, turn and enter the hard threats as they wish, which are unknown to the

TABLE 1. The desired heading angle and speed according to different cases.

Case	Desired Heading	Admissible Heading Range	Desired Speed	Admissible Speed Range
1	$\psi_{a,ms}(k)$	$\mathcal{V}_{\psi,s}(k)$	$V_s(k) + a_{s,min}\,\Delta t$	$\mathcal{V}_{V,s}(k)$
2	$\psi_{min,s}(k)$	$\mathcal{V}_{CAHR,s}(k)$	$V_s(k) + a_{s,min}\,\Delta t$	$\mathcal{V}_{V,s}(k)$
3	$\psi_{c,s}(k)$	$\mathcal{V}_{TAHR,s}(k)$	$V_s(k) + a_{s,max}\,\Delta t$	$\mathcal{V}_{V,s}(k)$
4	$\tan^{-1}\left(\frac{\alpha\,\sin(\psi_{c,s}(k))+\beta\,\sin(\psi_{min,s}(k))}{\alpha\,\cos(\psi_{c,s}(k))+\beta\,\cos(\psi_{min,s}(k))}\right)$	$\mathcal{V}_{TAHR,s}(k)$	$V_s(k) + K_V\,\Delta V_s(k) + K_r\,\frac{r_s(k)}{\Delta t}$	$\mathcal{V}_{V,s}(k)$

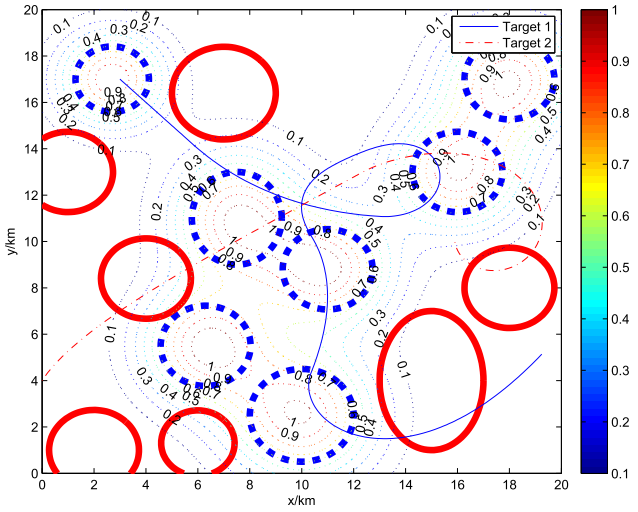

FIGURE 5. The threat environment and the true trajectories of the two targets. The solid circles are hard threats, the dashed circles are soft threats. The contour lines are the total soft threats according to Eq. (4). This same threat environment is used for all the simulation cases.

TABLE 2. The motion constraints of the UAVs.

Constraint	Minimum value	Maximum value
Speed (km/h)	72	180
Acceleration (m/s^2)	-2	2
Turning rate (degree/s)	-10	10

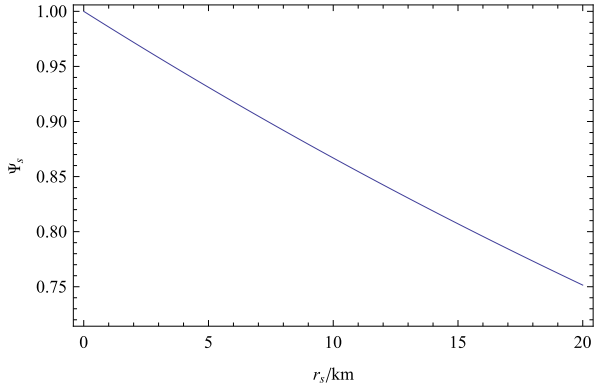

FIGURE 6. Detection probability versus sensor-target range when $r_0 = 70$ according to Eq. (12).

mission designers. The initial horizonal positions of the two targets are respectively $[3, 17]^T$ km and $[0, 4]^T$ km.

In the first 200 seconds target 1 accelerates from 0 to its maximum speed 144 km/h and then maintain the speed for 200 seconds. Then its speed decreases to 72 km/h at 800s and then increases to its maximum speed again at 1000s. In the remainder times the maximum speed is holding. Target 2 accelerates its speed from 36 km/h to 108 km/h in the first 300 seconds. After maintaining this speed for 200 seconds, target 2 stops from 700s to 900s. Then it accelerates to the maximum speed 144 km/h in 100 seconds which is kept till the end of the mission.

Without loss of generality and also to illustrate the results more conveniently, the same threat environment is assumed for all the UAVs in spite of different altitudes where they are flying. The threat environment and the true trajectories of the two targets are shown in Fig. 5.

There are 7 hard threats (red solid-line-bounded ellipse/circle) and 7 soft threats (blue dotted-line-bounded ellipse/circle). The contours are the total threat levels of all the soft threats according to Eq. (4).

Motion constraints of the UAVs are listed in Table 2.

And their initial speeds and heading angles are all set to be 108 km/h and 0 degree in all of the simulation experiments. At least two UAVs are allocated for each target at every time step (i.e., $\mathcal{K} \geq 2$). The reference range r_0 is selected as 70 km.

Figure 6 shows us how the detection probability changes with sensor-target range according to Eq. (6).

The designed parameters of the ANLSE method are set to be $\varepsilon = 0.001, L_{max} = 200, \varrho = 2.0$. To approximately determine the target trajectory the latest $L = 15$ position estimations for each target are used. The proportional gains K_V and K_r for *Case 4* are chosen to be 0.5 and 0.05, respectively, and the time constants of the first-order transfer functions for heading angle and speed responses are set to be 0.5 and 0.01 respectively. The soft threat threshold is set to be $\mathcal{G}_{TH}(\alpha) = \alpha + 0.1$. This choice results in the situation that no influence of the soft threats is considered when $\alpha = 1$ since the soft threat value of everywhere in the surveillance region is less than 1.1. The standoff distance R_{sf} and the closeness distance r_{TH} are taken as 0.5 km and 0.3 km respectively. The parameter ψ_0 in Eq. (32) is chosen as $3\pi/4$.

B. QUALITATIVE RESULTS

In the first experiment four UAVs initially at $[0, 6, 0.5]^T$, $[0.1, 8, 0.75]^T$, $[0.2, 18, 1.0]^T$ and $[0.1, 16, 1.25]^T$ respectively are used to follow the two targets given before. To see the efficiency of the proposed standoff multi-target following algorithm, the true trajectories of the targets are firstly used in this experiment. That is, the position estimation $\hat{\hat{\mathbf{p}}}_n(k)$ and the

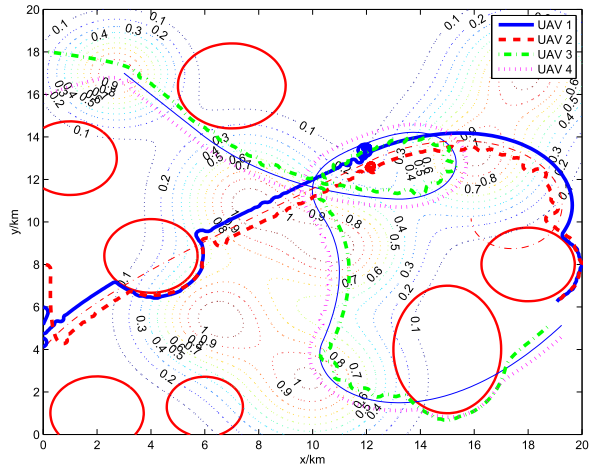

(a)

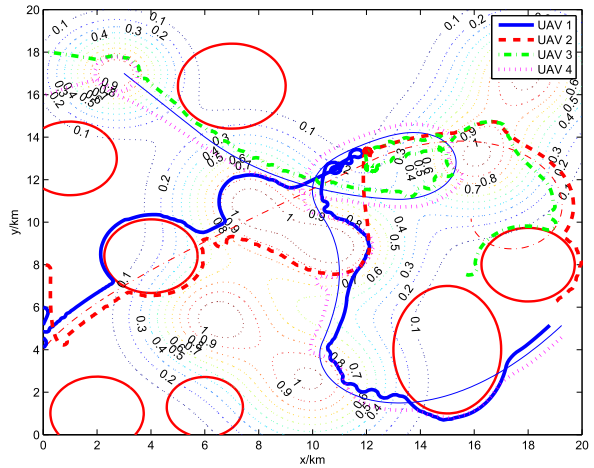

(b)

FIGURE 7. Standoff multi-target following with four UAVs using true trajectories of the targets: (a) $\alpha = 1.0$, (b) $\alpha = 0.8$.

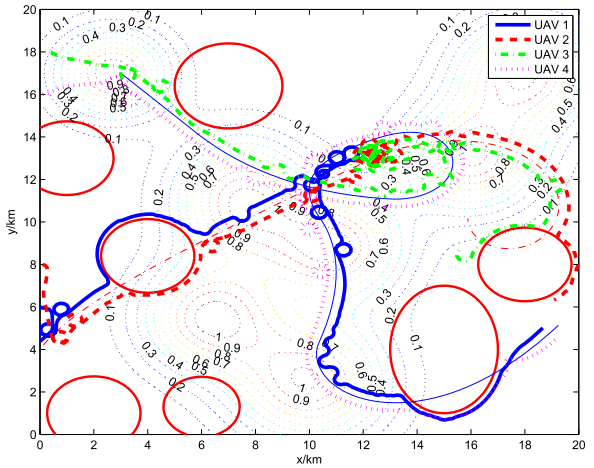

(a)

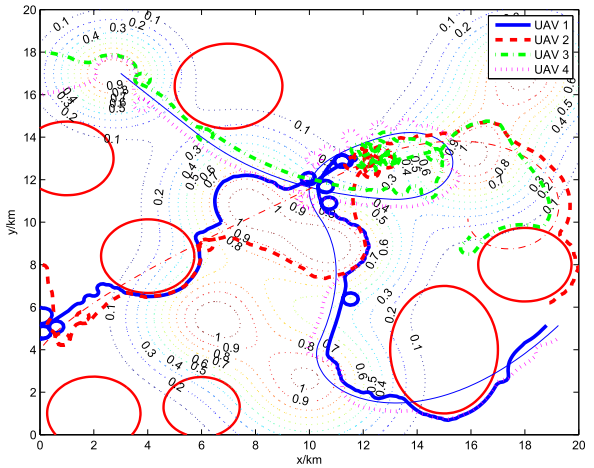

(b)

FIGURE 8. Standoff multi-target following with four UAVs using estimated trajectories of the targets when $\sigma_\mu = 1°$: (a) $\alpha = 1.0$, (b) $\alpha = 0.8$.

position and velocity predictions $\hat{\hat{\mathbf{p}}}_n(k+1|k)$ and $\hat{\hat{\mathbf{v}}}_n(k+1|k)$ (Eqns. (20), (26) and (27)) are replaced by the corresponding true values. The results are given in Fig. 7 when $\alpha = 1.0$ and $\alpha = 0.8$.

And the corresponding typical results using estimated trajectories are depicted in Fig. 8.

It can be seen that the UAVs can well follow the allocated targets as well as avoiding the collision with the hard threats and the access of the high-risk regions. Meanwhile the situation that certain UAVs may be far away from the allocated targets in the final times can also be noticed. This is because of the obstruction of the hard threats on one hand. On the other hand the time horizon (Δt herein) for task allocation and guidance turns out to be an important factor for the motion planning of UAVs [9]. Compared the results in Fig. 7 with those in Fig. 8, we can conclude the UAVs with the estimated target trajectories have to experience more frequent turns because of the inaccurate estimation. Figures 9 and 10 show us the comparison of the speeds and heading angles of UAV 1 in the first experiment using true and estimated target trajectories when $\alpha = 0.8$.

The results of the other UAVs with the other parameter α's are similar. The conclusion can be easily drawn from Fig. 9 that in the target following mission using estimated target trajectories the UAVs have to accelerate frequently and maintain the maximum speeds in comparatively long time which results in larger average speed. Figure 10 also gives us the argument that some unnecessary turns are done by the UAVs when estimated target trajectories are used.

Figure 11 gives us the estimation errors of the two targets corresponding to Fig. 8(b), from which we can see that the estimation errors are probably very large at the beginning of the mission and at the times when the targets enter some hard threats. Additionally the isolated spikes in the figure correspond to the times when the target is detected by only two sensors and when all of the NLSE iterations diverge.

In the second experiment an additional UAV initially staying at $[0, 11, 1.5]^T$ is assumed to be able to carry out the same

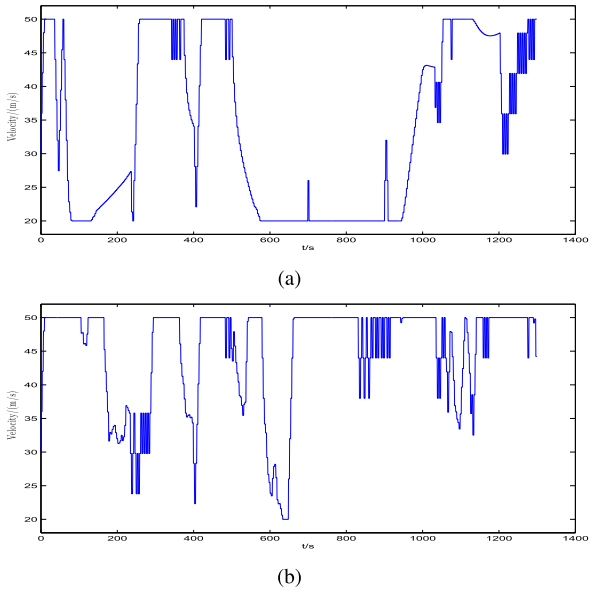

FIGURE 9. Speed comparison of UAV 1 with $\alpha = 0.8$ when (a) true trajectories and (b) estimated trajectories are used.

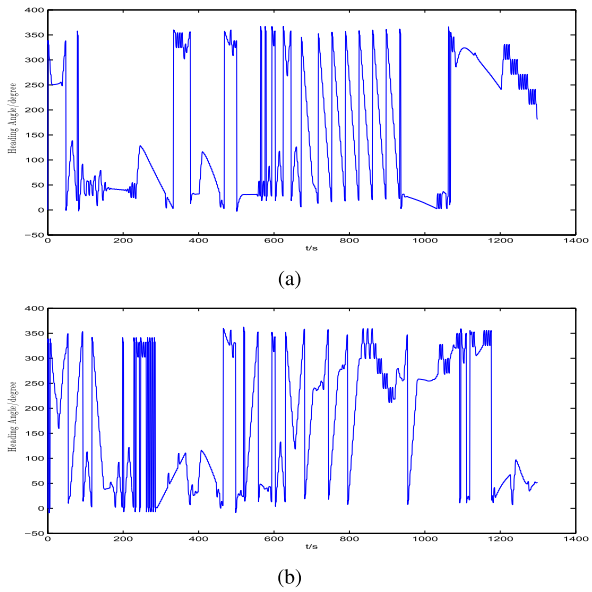

FIGURE 10. Heading angle comparison of UAV 1 with $\alpha = 0.8$ when (a) true trajectories and (b) estimated trajectories are used.

target following mission. Typical results of this experiment are shown in Fig. 12.

C. QUANTITATIVE RESULTS

Several metrics are developed here to assess the estimation and following efficiency.

The first one is the average root-mean-square error (ARMSE) which is widely used to exhibit the estimation performance.

The second one is called the total trajectory length ratio (TTLR), which is the total trajectory length of all the

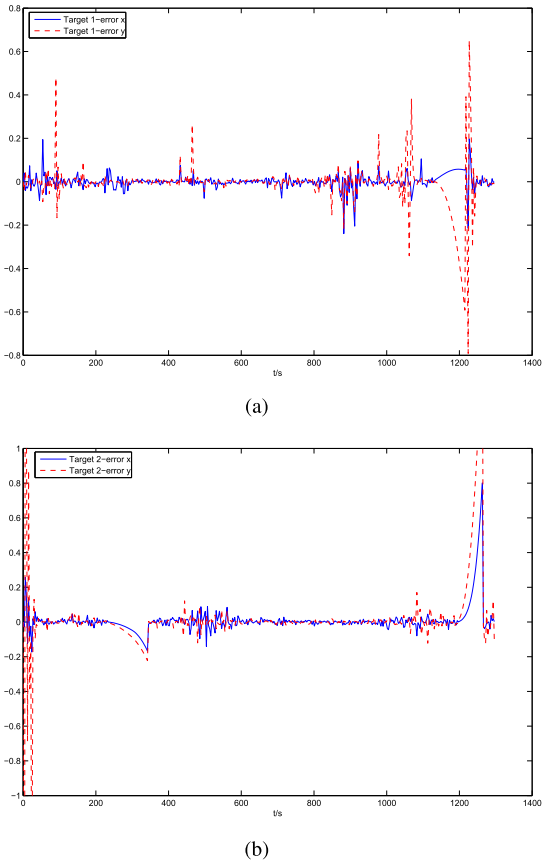

FIGURE 11. The estimation errors of (a) target 1 and (b) target 2 when $\alpha = 0.8$ and $\sigma_\mu = 1°$.

UAVs when estimated trajectories are used divided by the total trajectory length of all the UAVs when true trajectories are used. That is, the results when true trajectories are employed are used as criterions to assess the following efficiency. It is easy to see that if TTLR is closer to 1, then the following is better in the sense that the UAVs need not travel many unnecessary ways.

The third metric is introduced to see the conformity of the standoff following objective. We name this metric as average standoff distance (ASD). ASD of UAV s can be calculated as follows

$$\mathrm{ASD}_s = \frac{1}{K}\sum_{k=1}^{K}\sum_{n=1}^{N}\delta_{sn}(k)\left\|\mathbf{p}_s(k) - \tilde{\mathbf{p}}_n(k)\right\|, \qquad (51)$$

with K being the total simulation steps. The final ASD of all the UAVs is then

$$\mathrm{ASD} = \frac{1}{S}\sum_{s=1}^{S}\mathrm{ASD}_s. \qquad (52)$$

It obviously requires that ASD be as close to R_{sf} as possible.

To see if the allocated UAVs can follow every target with optimal geometric configuration, average angular spacing

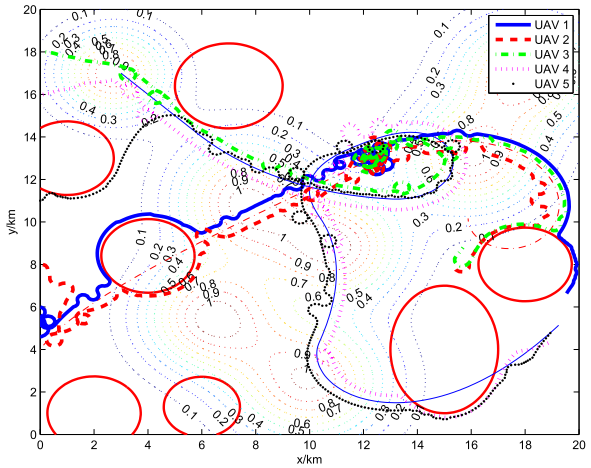

(a)

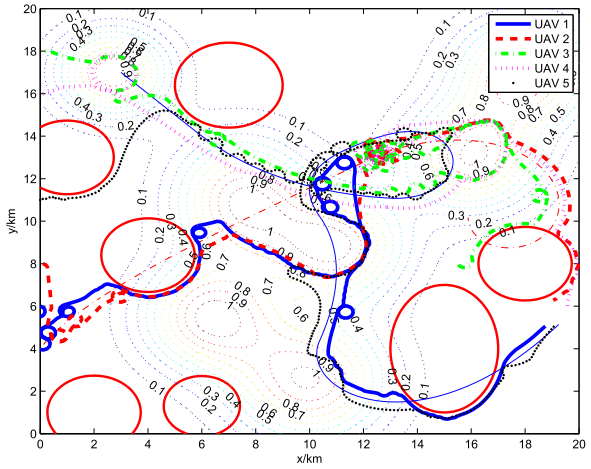

(b)

FIGURE 12. Standoff multi-target following with five UAVs using estimated trajectories of the targets when $\sigma_\mu = 1°$: (a) $\alpha = 1.0$, (b) $\alpha = 0.8$.

deviation (AASD) can be defined as

$$\mathrm{AASD}_n = \frac{1}{K}\sum_{k=1}^{K}\begin{cases}\sum_{i=1}^{S_n(k)-1}\left|\phi_{s_{i+1}}(k)-\phi_{s_i}(k)-\dfrac{2\pi}{S_n(k)}\right| \\ \text{if } S_n(k)>2 \\ \left|\phi_{s_2}(k)-\phi_{s_1}(k)-\dfrac{\pi}{S_n(k)}\right| \\ \text{if } S_n(k)=2 \text{ and } \phi_{s_2}(k)-\phi_{s_1}(k)\le\pi \\ \left|2\pi-\phi_{s_2}(k)+\phi_{s_1}(k)-\dfrac{\pi}{S_n(k)}\right| \\ \text{if } S_n(k)=2 \text{ and } \phi_{s_2}(k)-\phi_{s_1}(k)>\pi\end{cases} \tag{53}$$

for target n, where $S_n(k)$ is the number of UAVs assigned to follow target n at time t_k, and $\phi_{s_i}(k)$ is the azimuth of UAV s_i with respect to its allocated target at time t_k satisfying $\phi_{s_{i+1}}(k) \ge \phi_{s_i}(k)$ for i ranging from 1 to $S_n(k)-1$. And the final AASD can be taken as the average of all the targets.

TABLE 3. Simulation metrics of the first experiment with four UAVs.

Noise level	α	ARMSE 1	ARMSE 2	TTLR	ASD	AASD	PTTR
0	1	-	-	1	0.675	0.689	0.850
	0.9	-	-	1	0.773	0.660	0.762
	0.8	-	-	1	0.930	0.600	0.689
0.5°	1	0.965	1.048	1.306	0.782	0.684	0.830
	0.9	0.964	1.094	1.255	0.909	0.669	0.756
	0.8	1.004	1.240	1.216	1.022	0.641	0.654
1°	1	0.977	2.126	1.316	0.819	0.697	0.821
	0.9	0.981	2.220	1.265	0.950	0.686	0.743
	0.8	1.248	2.222	1.226	1.086	0.660	0.677
2°	1	1.307	3.912	1.328	0.884	0.726	0.835
	0.9	1.017	3.962	1.273	1.005	0.704	0.749
	0.8	1.537	3.920	1.233	1.107	0.677	0.648

TABLE 4. Simulation metrics of the second experiment with five UAVs.

Noise level	α	ARMSE 1	ARMSE 2	TTLR	ASD	AASD	PTTR
0	1	-	-	1	0.724	1.343	0.833
	0.9	-	-	1	0.808	1.318	0.752
	0.8	-	-	1	0.986	1.334	0.660
0.5°	1	0.969	1.105	1.279	0.824	1.319	0.817
	0.9	0.961	1.508	1.230	0.932	1.293	0.737
	0.8	0.986	1.008	1.220	1.074	1.252	0.640
1°	1	0.963	1.433	1.282	0.846	1.298	0.822
	0.9	0.969	1.395	1.234	0.939	1.279	0.730
	0.8	1.346	1.602	1.226	1.077	1.262	0.631
2°	1	1.640	1.557	1.293	0.936	1.305	0.829
	0.9	1.454	1.640	1.248	0.983	1.277	0.730
	0.8	1.187	1.639	1.234	1.128	1.239	0.637

It is assumed that when the relative UAV-target distance is not more than $1.8R_{sf}$, the allocated target is thought to be successfully tracked by a UAV. We then define the final metric, the persistent tracking time ratio (PTTR), as the average value of the ratios of all the UAVs of the time instants corresponding to the success time instants with the total simulation step K. This metric represents the persistent tracking capability of the UAVs.

Table 3 lists the simulation metrics of the first experiment with different noise levels (corresponding to different σ_μ's) and the parameter α's under 50 Monte Carlo evaluations. "ARMSE 1" and "ARMSE 2" in the table are respectively the position ARMSE of target 1 and target 2. Note that the noise level 0 corresponds to the simulations with true trajectories of the targets, and therefore it is meaningless to give the ARMSEs of this case, which is the same below.

The simulation metrics of the second experiment with different noise levels are given in Table 4.

From Tables 3-4 we can draw the conclusion that ARMSE will become larger as the noise level becomes bigger while the parameter α has no apparent influence on ARMSE. TTLR values of both the experiments stay in [1.2, 1.3]. Under the same noise level although the absolute trajectory lengths of all the UAVs are bigger with smaller α, the relative lengths to the results using true trajectories are smaller. The reason is that larger regions have to avoid when α is smaller and this relies much less on the estimated trajectories. As σ_μ gets larger, both of ASD value and AASD value tend to be larger.

This is easily to understand since the estimation gets worse. Smaller α leads to larger ASD value due to larger regions to avoid. Because the UAVs have to firstly fly close to the inaccurate positions of the allocated targets and avoid the hard threats and high-risk regions, the simulation values of ASD and AASD deviates relatively large from the ideal values (R_{sf} for ASD and 0 for AASD). The largest deviations of them exceeds 50%. It can be seen that for the same α value, there is no significant difference between the PTTR values of different noise levels.

D. COMPUTATIONAL BURDEN

Executing one step of the two experiments needs averagely 0.197s and 0.283s with the algorithm implemented in MATLAB 7.11.0 on a 3.40 GHz 2 CPU Pentium-based computer under Windows XP. Notice that $\Delta t = 3$s. Therefore we can say that the bearing-only standoff multi-target following mission can be accomplished online.

V. CONCLUSIONS AND FUTURE WORKS

The standoff multi-target following problem using multiple fixed-wing autonomous UAVs equipped with bearing sensors has been addressed in this paper. Taking consideration of the threat environment which involves in obstacles, restricted areas and air defence forces and sensor detection imperfection, the problem has been resolved real-timely by six steps. Simulation experiments are given to illustrate the solution of the whole mission.

In the noncooperative situation we choose to localize the targets and then approximate the target trajectories using quadratic functions of time t at every time step rather than assuming a set of multiple dynamic models for the targets. This bases on the two considerations below. The targets may undergo many maneuvers with different accelerations whose values are difficult to identify. In addition switches of different maneuvers may result in large model sets. This will then lead to large computation costs and difficulty of determining the mode transition matrices.

The parameter ψ_0 is kept constant during the whole mission in the simulation experiments. Actually ψ_0 can be adaptive according to the relative positions and velocities of the UAVs to the allocated targets. This can be used to avoid some unnecessary trajectory crossovers of different UAVs and reduce their speed changes, which result in energy saving for the UAVs. If the closeness parameter r_{TH} is too small, the UAVs will be in the state of *Case 3* for comparatively long time. The influence of this situation is that UAVs have to accelerate more frequently to get close to the allocated dummy targets, which leads to greater energy consumption.

The sensors in this paper are assumed to be omnidirectional ones. However in recent years, directional sensors such as ultrasound, infrared, and video sensors are used more and more. Directional sensors differ from omnidirectional ones in many aspects, such as angle of view, working direction, and line of sight (LoS) properties [38]. As we can imagine, interesting results can be obtained for path planning of directional sensor platforms. This will be our future focus of attention.

APPENDIX
CALCULATION OF $\psi_{a,ms}(k)$

We first take $\{\mathcal{A}_m(z_s), \mathcal{P}_m(z_s)\}$ as

$$\left\{\begin{bmatrix} a_x \\ a_y \end{bmatrix}, \begin{bmatrix} b_{11} & b_{12} \\ b_{12} & b_{22} \end{bmatrix}\right\}.$$

If $y_s(k) \neq a_y$, the intersection point $\mathbf{p}_\mathrm{i} = [x_\mathrm{i}, y_\mathrm{i}]^T$ can be computed as

$$\begin{aligned} y_\mathrm{i} &= a_y + \frac{\left(y_s(k) - a_y\right)\sqrt{b_{11}b_{22} - b_{12}^2}}{\sqrt{\Gamma}}, \\ x_\mathrm{i} &= a_x + \frac{\left(x_s(k) - a_x\right)\left(y_\mathrm{i} - a_y\right)}{\left(y_s(k) - a_y\right)}, \end{aligned} \tag{54}$$

where

$$\begin{aligned} \Gamma = {} & b_{22}\left(x_s(k) - a_x\right)^2 + b_{11}\left(y_s(k) - a_y\right)^2 \\ & - 2b_{12}\left(x_s(k) - a_x\right)\left(y_s(k) - a_y\right). \end{aligned} \tag{55}$$

And if $y_s(k) = a_y$, we have

$$\begin{aligned} y_\mathrm{i} &= a_y, \\ x_\mathrm{i} &= \begin{cases} a_x + \sqrt{\frac{b_{11}b_{22} - b_{12}^2}{b_{22}}}, & \text{if } x_s(k) \geq a_x \\ a_x - \sqrt{\frac{b_{11}b_{22} - b_{12}^2}{b_{22}}}, & \text{otherwise} \end{cases} \end{aligned} \tag{56}$$

The two perpendicular directions of the tangential at the intersection point $\mathbf{p}_\mathrm{i}$ are given by

$$\psi_{a,ms}^{\pm}(k) = \tan^{-1}\left(\frac{\pm\left[b_{11}\left(y_\mathrm{i} - a_y\right) - b_{12}\left(x_\mathrm{i} - a_x\right)\right]}{\pm\left[b_{22}\left(x_\mathrm{i} - a_x\right) - b_{12}\left(y_\mathrm{i} - a_y\right)\right]}\right), \tag{57}$$

and then the one which is closer to the direction of vector $\overrightarrow{\mathcal{A}_m(z_s)\mathbf{p}_s(k)}$ is taken as $\psi_{a,ms}(k)$.

REFERENCES

[1] U. Zengin and A. Dogan, "Real-time target tracking for autonomous UAVs in adversarial environments: A gradient search algorithm," *IEEE Trans. Robot.*, vol. 23, no. 2, pp. 294–307, Apr. 2007.

[2] T. H. Summer, M. R. Akella, and M. J. Mears, "Coordinated standoff tracking of moving targets: Control laws and information architectures," *J. Guid.. Control, Dyn.*, vol. 32, no. 1, pp. 56–69, Jan./Feb. 2009.

[3] Y. V. Pehlivanoglu, "A new vibrational genetic algorithm enhanced with a Voronoi diagram for path planning of autonomous UAV," *Aerosp. Sci. Technol.*, vol. 16, no. 1, pp. 47–55, Jan./Feb. 2012.

[4] C. Xu, H. Duan, and F. Liu, "Chaotic artificial bee colony approach to Uninhabited Combat Air Vehicle (UCAV) path planning," *Aerosp. Sci. Technol.*, vol. 14, no. 8, pp. 535–541, Dec. 2010.

[5] L. F. Bertuccelli and J. P. How, "UAV search for dynamic targets with uncertain motion models," in *Proc. IEEE Conf. Decision Control (CDC)*, Dec. 2006, pp. 5941–5946.

[6] L. F. Bertuccelli and J. P. How, "Search for dynamic targets with uncertain probability maps," in *Proc. Amer. Control Conf. (ACC)*, Jun. 2006, pp. 737–742.

[7] R. R. Pitre, X. R. Li, and R. Delbalzo, "UAV route planning for joint search and track missions—An information-value approach," *IEEE Trans. Aerosp. Electron. Syst.*, vol. 48, no. 3, pp. 2551–2565, Jul. 2012.

[8] J. R. Riehl, G. E. Collins, and J. P. Hespanha, "Cooperative search by UAV teams: A model predictive approach using dynamic graphs," *IEEE Trans. Aerosp. Electron. Syst.*, vol. 47, no. 4, pp. 2637–2656, Oct. 2011.
[9] J. Ousingsawat and M. E. Campbell, "Optimal cooperative reconnaissance using multiple vehicles," *J. Guid., Control, Dyn.*, vol. 30, no. 1, pp. 122–132, Jun./Feb. 2007.
[10] N. Ceccarelli, J. J. Enright, E. Frazzoli, S. J. Rasmussen, and C. J. Schumacher, "Micro UAV path planning for reconnaissance in wind," in *Proc. Amer. Control Conf. (ACC)*, Jul. 2007, pp. 5310–5315.
[11] E. W. Frew, D. A. Lawrence, and S. Morris, "Coordinated standoff tracking of moving targets using Lyapunov guidance vector fields," *J. Guid., Control, Dyn.*, vol. 31, no. 2, pp. 290–306, Mar./Apr. 2008.
[12] X. C. Ding, A. R. Rahmani, and M. Egerstedt, "Multi-UAV convoy protection: An optimal approach to path planning and coordination," *IEEE Trans. Robot.*, vol. 26, no. 2, pp. 256–268, Apr. 2010.
[13] S. Martínez, F. Bullo, "Optimal sensor placement and motion coordination for target tracking," *Automatica*, vol. 42, no. 4, pp. 661–668, Apr. 2006.
[14] A. N. Bishop, B. Fidan, B. D. O. Anderson, K. Doğançay, and P. N. Pathirana, "Optimality analysis of sensor-target localization geometries," *Automatica*, vol. 46, no. 3, pp. 479–492, Mar. 2010.
[15] K. Doğançay, "UAV path planning for passive emitter localization," *IEEE Trans. Aerosp. Electron. Syst.*, vol. 48, no. 2, pp. 1150–1166, Apr. 2012.
[16] O. Hachour, "Path planning of autonomous mobile robot," *Int. J. Syst. Appl., Eng. Develop.*, vol. 2, no. 4, pp. 178–190, 2008.
[17] P. Bhattacharya and M. L. Gavrilova, "Roadmap-based path planning—Using the voronoi diagram for a clearance-based shortest path," *IEEE Robot. Autom. Mag.*, vol. 15, no. 2, pp. 58–66, Jun. 2008.
[18] S. A. Bortoff, "Path planning for UAVs," in *Proc. Amer. Control Conf.*, Jun. 2000, pp. 364–368.
[19] J. Barraquand, B. Langlois, and J.-C. Latombe, "Numerical potential field techniques for robot path planning," *IEEE Trans. Syst., Man, Cybern.*, vol. 22, no. 2, pp. 224–241, Mar./Apr. 1992.
[20] Y.-B. Chen, G.-C. Luo, Y.-S. Mei, J.-Q. Yu, and X.-L. Su, "UAV path planning using artificial potential field method updated by optimal control theory," *Int. J. Syst. Sci.*, vol. 47, no. 6, pp. 1407–1420, 2016.
[21] V. Roberge, M. Tarbouchi, and G. Labonte, "Comparison of parallel genetic algorithm and particle swarm optimization for real-time UAV path planning," *IEEE Trans Ind. Informat.*, vol. 9, no. 1, pp. 132–141, Feb. 2013.
[22] H. Duan and P. Qiao, "Pigeon-inspired optimization: A new swarm intelligence optimizer for air robot path planning," *Int. J. Intell. Comput. Cybern.*, vol. 7, no. 1, pp. 24–37, Mar. 2014.
[23] S. M. LaValle, *Planning Algorithms*. London, U.K.: Cambridge Univ. Press, 2006.
[24] C. Goerzen, Z. Kong, and B. Mettler, "A survey of motion planning algorithms from the perspective of autonomous UAV guidance," *J. Intell. Robot. Syst.*, vol. 57, no. 1, pp. 65–100, Jan. 2009.
[25] P. Raja and S. Pugazhenthi, "Optimal path planning of mobile robots: A review," *Int. J. Phys. Sci.*, vol. 7, no. 9, pp. 1314–1320, Feb. 2012.
[26] C. Schumacher, "Ground moving target engagement by cooperative UAVs," in *Proc. Amer. Control Conf. (ACC)*, Jun. 2005, pp. 4502–4505.
[27] U. Zengin and A. Dogan, "Cooperative target pursuit by multiple UAVs in an adversarial environment," *Robot. Auton. Syst.*, vol. 59, no. 12, pp. 1049–1059, Dec. 2011.
[28] R. A. Wise and R. T. Rysdyk, "UAV coordination for autonomous target tracking," in *Proc. AIAA Guid. Navig. Control Conf. Exhib. (GNCC)*, Aug. 2006, p. 6453.
[29] K. R. Pattipati, S. Deb, Y. Bar-Shalom, and R. B. Washburn, "A new relaxation algorithm and passive sensor data association," *IEEE Trans. Autom. Control*, vol. 37, no. 2, pp. 197–213, Feb. 1992.
[30] S. Deb, M. Yeddanapudi, K. Pattipati, and Y. Bar-Shalom, "A generalized S-D assignment algorithm for multisensor-multitarget state estimation," *IEEE Trans. Aerosp. Electron. Syst.*, vol. 33, no. 2, pp. 523–538, Apr. 1997.
[31] T. Sathyan, A. Sinha, and T. Kirubarajan, "Passive geolocation and tracking of an unknown number of emitters," *IEEE Trans. Aerosp. Electron. Syst.*, vol. 42, no. 2, pp. 740–750, Apr. 2006.
[32] T. Sathyan, A. Sinha, T. Kirubarajan, M. McDonald, and T. Lang, "MDA-based data association with prior track information for passive multitarget tracking," *IEEE Trans. Aerosp. Electron. Syst.*, vol. 47, no. 1, pp. 539–556, Jan. 2011.
[33] D. P. Bertsekas, *Linear Network Optimization: Algorithms and Codes*. Cambridge, MA, USA: MIT Press, 1991.
[34] J. T. Betts, "Survey of numerical methods for trajectory optimization," *J. Guid., Control, Dyn.*, vol. 21, no. 2, pp. 193–207, Mar./Apr. 1998.
[35] D. Benson, "A gauss pseudospectral transcription for optimal control," Ph.D. dissertation, Dept. Aeronautics Astronautics, Massachusetts Inst. Technol., Cambridge, MA, USA, 2004.
[36] G. T. Huntington, "Advancement and analysis of Gauss pseudospectral transcription for optimal control problems," Ph.D. dissertation, Dept. Aeronautics Astronautics, Massachusetts Inst. Technol., Cambridge, MA, USA, 2007.
[37] D. Garg *et al.*, "A unified framework for the numerical solution of optimal control problems using pseudospectral methods," *Automatica*, vol. 46, no. 11, pp. 1843–1851, 2010.
[38] M. Amac Guvensan and A. Gokhan Yavuz, "On coverage issues in directional sensor networks: A survey," *Ad Hoc Netw.*, vol. 9, no. 7, pp. 1238–1255, 2011.

HAO JIANG received the B.S. degree in control theory and applications from Beihang University, Beijing, China, in 2010, where he is currently pursuing the Ph.D. degree in applied mathematics. His current research interests include event-triggered control systems and path planning using unmanned aerial vehicles.

YUEQIAN LIANG was born in Shandong, China. He received the B.S. degree in information and computation science from the Minzu University of China, Beijing, China, in 2008, and the Ph.D. degree in control theory and applications from Beihang University, Beijing, in 2017. His current research interests include target tracking using unmanned aerial vehicles.